12

Modeling and Characterization of Power Generation Modules Based on Bulk Materials

Timothy P. Hogan and Tom Shih
Michigan State University

12.1 Introduction

In 1931, Onsager[1] described the set of general linear equations, often called the thermodynamic equations of motion, which gave a macroscopic description of flows of particles or of energy as being driven by various thermodynamic forces. He observed that for most processes of interest, the flow is directly proportional to the corresponding force that drives it. Common examples cited include heat transfer where the vector flow of energy is proportional to the temperature gradient, or Ohm's law in which the electrical current density is proportional to the voltage gradient. Onsager suggested that each of the flows, $\mathbf{J}_i$, in a given steady-state system is proportional to the sum of all forces, $\mathbf{X}_j$, acting on the system. This can be written generally as

$$\mathbf{J}_i = \sum_j L_{ij}\mathbf{X}_j \tag{12.1}$$

In a three-flow system, the flows would be written as

$$\begin{aligned} \mathbf{J}_1 &= L_{11}\mathbf{X}_1 + L_{12}\mathbf{X}_2 + L_{13}\mathbf{X}_3 \qquad \mathbf{J}_2 = L_{21}\mathbf{X}_1 + L_{22}\mathbf{X}_2 + L_{23}\mathbf{X}_3 \\ \mathbf{J}_3 &= L_{31}\mathbf{X}_1 + L_{32}\mathbf{X}_2 + L_{33}\mathbf{X}_3 \end{aligned} \tag{12.2}$$

These macroscopic quantities can be related to the microscopic properties of the materials through the L_{ij} parameters. In the case of thermoelectric (TE) materials, a two-flow system including electrical current

flow **J**, and heat flow **q** (as fluxes), and the forces of potential gradient ∇V, and temperature gradient ∇T, or

$$\mathbf{J} = L_{11}\nabla V + L_{12}\nabla T \qquad \mathbf{q} = L_{21}\nabla V + L_{22}\nabla T \tag{12.3}$$

Ohm's law is given by $\mathbf{J} = \sigma\mathbf{E} = -\sigma\nabla V$ for an isothermal sample ($\nabla T = 0$) with electrical conductivity σ and the heat flux is $\mathbf{q} = -\kappa\nabla T$ for a sample with no electric fields present. For inhomogeneous samples or when temperature gradients are present, then variations in the chemical potential μ, as well as the electrostatic potential V, must be included in the potential gradient. The forces and flows given in Equation 12.3 can be rewritten in terms of particle current density $\mathbf{J}_q$ and entropy current density $\mathbf{J}_s$, as

$$\mathbf{J}_q = -L_{qq}\nabla\bar{\mu} - L_{qs}\nabla T \qquad \mathbf{J}_s = -L_{qs}\nabla\bar{\mu} - L_{ss}\nabla T \tag{12.4}$$

where $\bar{\mu} = \mu + eV$ is the electrochemical potential. The heat current density (or heat flux) and energy current density (or energy flux) are given by

$$\mathbf{q} = T\mathbf{J}_s \qquad \mathbf{W} = \mathbf{q} + \bar{\mu}\mathbf{J}_q \tag{12.5}$$

For charge carriers being electrons, $e = -1.602 \times 10^{-19}$ Coulombs, and

$$L_{qq} = \frac{\sigma}{e^2} = \frac{1}{e^2\rho} \qquad T\left(\frac{L_{qq}L_{ss} - L_{qs}^2}{L_{qq}}\right) = \kappa \qquad \frac{L_{qs}}{L_{qq}} = S^* = e\alpha \tag{12.6}$$

where ρ is the electrical resistivity, κ is the thermal conductivity, S^* is the transport entropy per particle, and α is the TE power (or absolute Seebeck coefficient). Combining Equation 12.4, Equation 12.5, and Equation 12.6 gives

$$\mathbf{J}_s = S^*\mathbf{J}_q - \frac{\kappa}{T}\nabla T \tag{12.7}$$

$$\mathbf{W} = (TS^* + \bar{\mu})\mathbf{J}_q - \kappa\nabla T \tag{12.8}$$

$$\nabla\bar{\mu} = -e^2\rho\mathbf{J}_q - S^*\nabla T \tag{12.9}$$

Equation 12.8 shows the total energy current density has contributions from entropy and particle transport, while Equation 12.9 can be viewed as a generalized Ohm's law, which under isothermal ($\nabla T = 0$) and chemically homogenous ($\nabla\bar{\mu} = e\nabla V$) conditions reduces to the normal Ohm's law ($\nabla V = -e\rho\mathbf{J}_q$).

There can be no accumulation of energy within an infinitesimal volume; therefore, the total energy current density **W**, given in Equation 12.8, must have zero divergence. For the one-dimensional case, this leads to Domenicali's equation[2] for energy balance

$$\frac{\partial}{\partial x}\left(\kappa(x)\frac{\partial T(x)}{\partial x}\right) = -\rho J^2 + JT(x)\frac{\partial\alpha(x)}{\partial x} \tag{12.10}$$

and the equation of heat flux

$$q(x) = JT(x)\alpha(x) - \kappa(x)\frac{\partial T(x)}{\partial x} \tag{12.11}$$

12.2 Modeling Techniques

12.2.1 Exact

An analytically exact technique has been described by Sherman, Heikes, and Ure[3] for a p–n couple in the configuration described in Figure 12.1.

In this technique the efficiency is determined by setting up the governing equations for the full generator, such that Equation 12.11 is written to include the n- and p-contributions as

$$Q_h = IT_h[\alpha_p(T_h) - \alpha_n(T_h)] - \kappa_p(T_h)\frac{dT_p}{dx}\bigg|_{x=0} - A_n\kappa_n(T_h)\frac{dT_n}{dx}\bigg|_{x=0} \tag{12.12}$$

where the cross-sectional area of the p-leg is assumed equal to 1 cm^2 and the cross-sectional area of the n leg is A_n. In the actual device, the cross-sectional are of the p-leg is not, in general, equal to 1 cm^2; however, if the ratio of cross-sectional areas between the p- and n-legs remains constant, then there is no change in the efficiency. Equation 12.12 can be inserted into the formula for thermodynamic efficiency $\eta_t = P_o/Q_h$, along with the output power, $P_o = I^2R_L$, where the electrical current is given by the open circuit voltage divided by the total resistance, or

$$I = \frac{\int_{T_c}^{T_h}[\alpha_p(T) - \alpha_n(T)]dT}{R_L + \int_0^L\left[\rho_p(T) + \frac{\rho_n(T)}{A_n}\right]dx} \tag{12.13}$$

The load resistance, R_L, can be eliminated from the equation by rearranging Equation 12.13 as

$$I\left\{R_L + \int_0^L\left[\rho_p(T) + \frac{\rho_n(T)}{A_n}\right]dx\right\} = \int_{T_c}^{T_h}[\alpha_p(T) - \alpha_n(T)]dT \tag{12.14}$$

and subtracting the necessary components to obtain the electrical output power as

$$I^2R_L = I\left[\int_{T_c}^{T_h}[\alpha_p(T) - \alpha_n(T)]dT\right] - I^2\left[\int_0^L\left[\rho_p(T) + \frac{\rho_n(T)}{A_n}\right]dx\right] \tag{12.15}$$

The efficiency can then be written as

$$\eta_t = \frac{\int_{T_c}^{T_h}[\alpha_p(T) - \alpha_n(T)]dT - I\left[\int_0^L\left[\rho_p(T) + \frac{\rho_n(T)}{A_n}\right]dx\right]}{T_h[\alpha_p(T_h) - \alpha_n(T_h)] - \frac{\kappa_p(T_h)}{I}\frac{dT_p}{dx}\Big|_{x=0} - \frac{A_n\kappa_n(T_h)}{I}\frac{dT_n}{dx}\Big|_{x=0}} \tag{12.16}$$

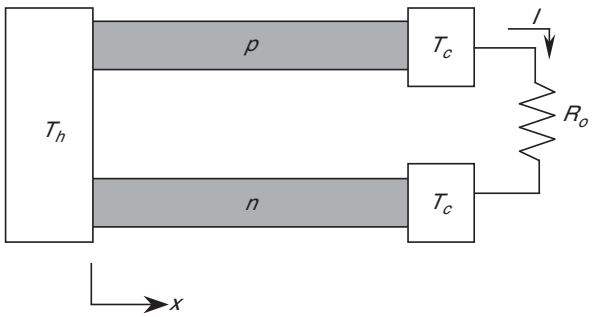

FIGURE 12.1 Single couple TE generator and coordinate system for the exact modeling technique. (*Source*: Sherman, B., Heikes, R.R., and Ure, R.W. Jr., *J. Appl. Phys.*, 31(1), 1–16, 1960. With permission.)

Using, $J_p = I$, and $J_n A_n = -I$ gives

$$\eta_t = \frac{\int_{T_c}^{T_h} [\alpha_p(T) - \alpha_n(T)]dT - J_p \int_0^L \rho_p(T)dx + J_n \int_0^L \rho_n(T)dx}{T_h[\alpha_p(T_h) - \alpha_n(T_h)] - \frac{\kappa_p(T_h)}{J_p}\frac{dT_p}{dx}\Big|_{x=0} + \frac{\kappa_n(T_h)}{J_n}\frac{dT_n}{dx}\Big|_{x=0}} \tag{12.17}$$

This can be simplified through a change of variable:

$$y_n(T) = -\frac{\kappa_n(T)}{J_n \frac{dx_n}{dT}} \qquad \text{and} \qquad y_p(T) = -\frac{\kappa_p(T)}{J_p \frac{dx_p}{dT}} \tag{12.18}$$

such that

$$\frac{dy_n(T)}{dT} = -\tau_n(T) - \frac{\rho_n \kappa_n(T)}{y_n(T)} \tag{12.19}$$

where $\tau_n(T) = T\frac{d\alpha_n(T)}{dT}$ is the Thomson coefficient for the n-leg, and the electrical current density can be written as

$$J_n L = \int_{T_c}^{T_h} \frac{\kappa_n(T)}{y_n(T)} dT = -\int_{T_c}^{T_h} J_n \frac{dx_n}{dT} dT \tag{12.20}$$

where L is the full length of the n leg. Using a similar procedure for the p-leg, the efficiency for the p–n couple is

$$\eta_t = \frac{Q_h - Q_c}{Q_h} = 1 - \frac{y_p(T_c) - y_n(T_c) + T_c[\alpha_p(T_c) - \alpha_n(T_c)]}{y_p(T_h) - y_n(T_h) + T_h[\alpha_p(T_h) - \alpha_n(T_h)]} \tag{12.21}$$

In determining the maximum efficiency with this method, trial values for $y_p(T_h)$ and $y_n(T_h)$ are approximated. Then $y_p(T)$ and $y_n(T)$ are determined by numerical integration of Equation 12.18, and the efficiency η, is calculated by Equation 12.21. This procedure is repeated for more trial values of $y_p(T_h)$ and $y_n(T_h)$ until a maximum in the efficiency is found. The values of J_p and J_n are then determined by the functions $y_p(T)$ and $y_n(T)$ that yield the maximum efficiency, and the integration of Equation 12.20.

The thermal efficiency given in Equation 12.17 for the module can also be written in terms of the efficiencies of the individual legs as

$$\eta_t = \frac{\int_{T_c}^{T_h} \alpha_p(T)dT - J_p \int_0^L \rho_p(T)dx - \int_{T_c}^{T_h} \alpha_n(T)dT + J_n \int_0^L \rho_n(T)dx}{T_h[\alpha_p(T_h)] - \frac{\kappa_p(T_h)}{J_p}\frac{dT_p}{dx}\Big|_{x=0} - T_h[\alpha_n(T_h)] + \frac{\kappa_n(T_h)}{J_n}\frac{dT_n}{dx}\Big|_{x=0}}$$

$$= \frac{\eta_p\left(\frac{q_{h_p}}{J_p}\right) - \eta_n\left(\frac{q_{h_n}}{J_n}\right)}{\left(\frac{q_{h_p}}{J_p}\right) - \left(\frac{q_{h_n}}{J_n}\right)} \tag{12.22}$$

where q_{h_p} and q_{h_n} are the heat flow densities (in W/cm^2) into the hot-sides of the p-type and n-type legs, respectively. For the x direction defined in Figure 12.1, $J_p = I$, and $J_n A_n = -I$; therefore

$$\eta_t = \frac{\eta_p(Q_{h_p}) + \eta_n(Q_{h_n})}{Q_{h_p} + Q_{h_n}} \tag{12.23}$$

where Q_{h_p} and Q_{h_n} are the heat flows (in watts) into the hot-sides of the p-type and n-type legs, respectively.

12.2.2 Iterative

In the iterative technique[4,5] a single leg (n-type or p-type) of the TE device is mathematically subdivided into many small segments such that there is a correspondingly small temperature gradient across each segment. In this condition, the material properties of α, ρ, and κ for a given segment are assumed to be constant over the small temperature gradient across that segment. Equation 12.10 and Equation 12.11 can be rearranged into a coupled set of first-order equations[6] as

$$\frac{dT(x)}{dx} = \frac{1}{\kappa(x)}[JT(x)\alpha(x) - q(x)] \tag{12.24}$$

and

$$\frac{dq(x)}{dx} = \rho(x)J^2[1 - Z(x)T(x)] - \frac{J\alpha(x)q(x)}{\kappa(x)} \tag{12.25}$$

For $dx \rightarrow 0$ Equation 12.24 and Equation 12.25 can be written for the first segment as:

$$T_1 = T_0 + \frac{dx}{\kappa_0}[JT_0\alpha_0 - q_0] \tag{12.26}$$

$$q_1 = q_0 + \left[\rho_0 J^2\left(1 - \frac{\alpha_0^2 T_0}{\rho_0\kappa_0}\right) - \frac{J\alpha_0 q_0}{\kappa_0}\right]dx \tag{12.27}$$

The output from one segment of the leg becomes the input for the adjacent segment, such that an iterative method can be used for determining the correct heat flow and temperature profile such as:

1. Begin with a guess of q_0 for the cold-side of the leg (at temperature T_0).
2. Use the values of T_0 and q_0 to calculate T_1 and q_1 from Equation 12.26 and Equation 12.27, and the material properties of the leg at the temperature T_0.
3. Repeat this procedure for calculating T_2 and q_2 from T_1 and q_1, and the material properties of the leg at the temperature T_1. Continue for each segment up to the final segment at T_N and q_N.
4. If T_N is not equal to the hot-side temperature, then chose a new guess value for q_0 and start the procedure over again.
5. Continue this iterative process until T_N is equal to the desired hot-side temperature.

This is repeated for the other leg of the module. The efficiency of the n-type leg can then be determined as

$$\eta_n = \frac{J_n\left(\int_0^L \alpha_n(x)\frac{dT(x)}{dx}dx + J_n\int_0^L \rho(x)dx\right)}{q_{h_n}} \tag{12.28}$$

and similarly for the p-type leg (under normal operation q_{h_p}, q_{h_n}, and J_p are negative quantities for the x direction defined in Figure 12.2).

To determine the maximum module efficiency based on η_n and η_p, Equation 12.23 is maximized. This iterative technique was tested for the examples given in Ref. [3], with material properties described in Table 12.1. The module for Example I is for a temperature gradient of T_c =400 K and T_h = 750 K, while Examples II and III (fictitious materials) have T_c = 400 K and T_h = 1500 K.

The cross-sectional area of the p-type leg is assumed equal to 1 cm^2. The optimal cross-sectional area for the n-type leg is then determined as described below, such that the ratio of areas is known. The cross-sectional areas can be varied without degradation to the maximum efficiency as long as this

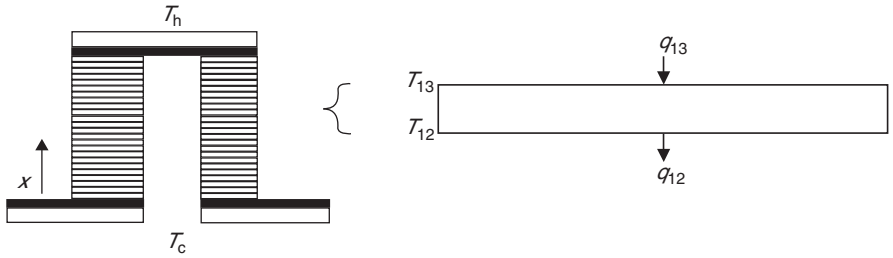

FIGURE 12.2 Mathematical segmentation of each leg of a TE module. Equation 12.26 and Equation 12.27 are applied to each segment and iteratively solved from the cold to the hot end until the desired temperature profile is obtained and the heat flow determined.

TABLE 12.1 TE Properties for Example Modules Described in Ref. [3]

	σ (S/cm)	α (μV/K)	κ (W/cm K)
Example I (n-type)	$\sigma_n = \frac{T-310}{0.1746}$	$\alpha_n = 0.268 \cdot T - 329$	$\kappa_n = \frac{54}{T}$
Example I (p-type)	$\sigma_p = 25$	$\alpha_p = 0.150 \cdot T + 211$	$\kappa_p = \frac{3.194}{T}$
Example II (n-type)	$\sigma_n = \frac{10^5}{T}$	$\alpha_n = 0.20 \cdot T - 400$	$\kappa_n = \frac{3}{T}$
Example II (p-type)	$\sigma_p = T$	$\alpha_p = 200$	$\kappa_p = \frac{10}{T}$
Example III (n-type)	$\sigma_n = 1000$	$\alpha_n = 0.20 \cdot T$	$\kappa_n = \frac{3}{T}$
Example III (p-type)	$\sigma_p = T$	$\alpha_p = 200$	$\kappa_p = \frac{10}{T}$

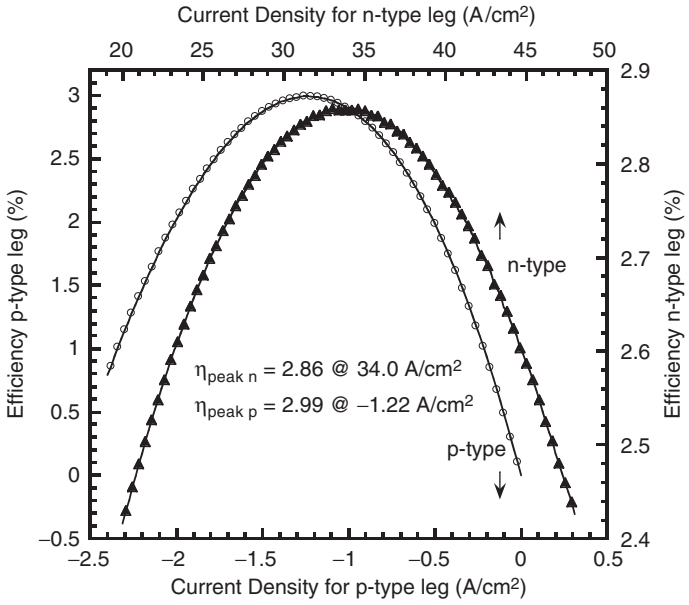

FIGURE 12.3 Efficiencies for the n-type and p-type legs of Example I.

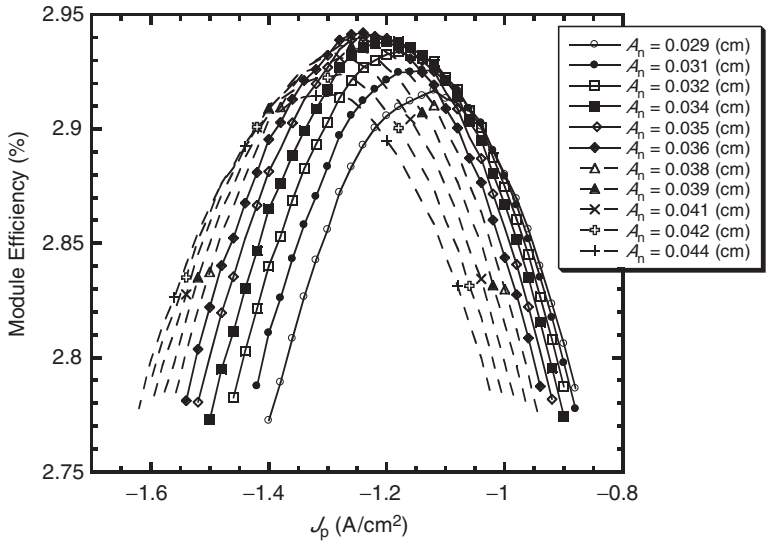

FIGURE 12.4 Efficiency vs. J_p for various A_n values for Example I module.

ratio remains constant. Results for Example I materials give individual leg efficiencies as shown in Figure 12.3, and Figure 12.4. For Example II there is a larger shift from the peak of η_p for the maximum efficiency of the module η_t, as shown in Figure 12.5, Figure 12.6, and Figure 12.7. The temperature profiles along the leg and heat flux through the n-type and p-type legs obtained from the iterative technique is shown in Figure 12.8.

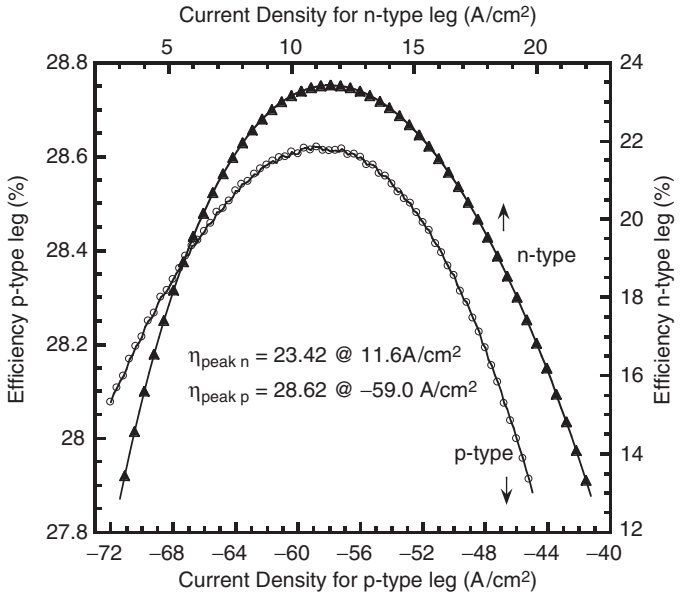

FIGURE 12.5 Efficiencies for the n-type and p-type legs of Example II.

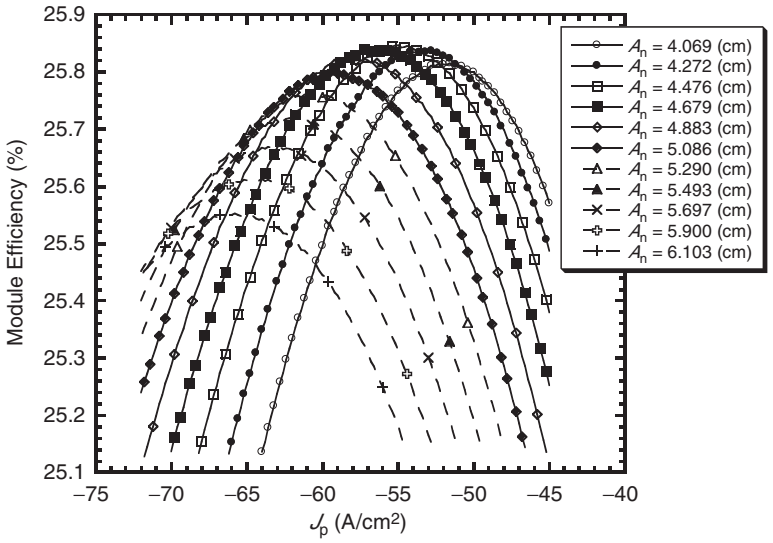

FIGURE 12.6 Efficiency vs. J_p for various A_n values for Example II module.

A comparison between results from the iterative technique and the exact approach for the three examples given in Ref. [3] are listed in Table 12.2.

Agreement between the modeling techniques is found to improve with finer current density steps and smaller values of dx in Equation 12.26 and Equation 12.27.

The iterative technique is also applicable to modules with segmented legs consisting of multiple n-type materials and/or multiple p-type materials. A test example found in Ref. [7] was used for a segmented structure. In this reference, the module efficiency is found by using the average material properties over the temperature gradient of a specific segment of the leg. The module consists of a p-type leg with three segments (P_1, P_2, and P_3) and an n-type leg with two segments (N_1 and N_2). The material properties are taken as temperature independent with values given in Table 12.3.

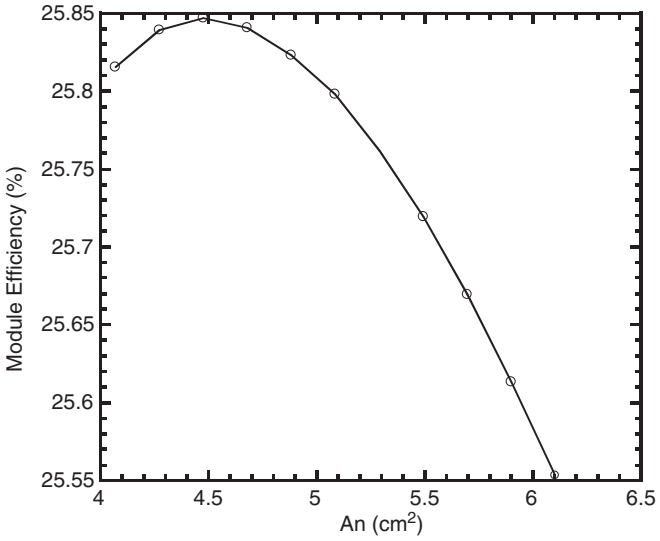

FIGURE 12.7 Module thermal efficiency, η_t, vs. A_n for Example II module.

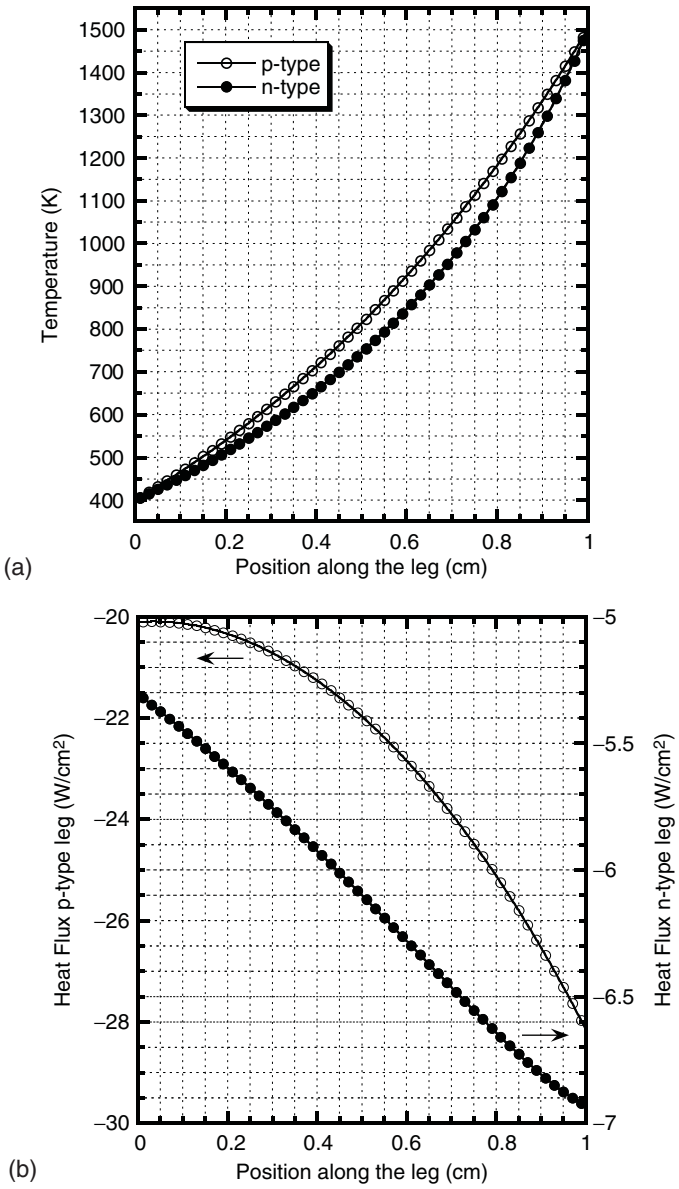

FIGURE 12.8 Temperature profiles (a) and heat flux (b), q_n and q_p, on the n-type and p-type legs for the Example II module.

A comparison of the results from the iterative technique and the results given in Ref. [7] are shown in Table 12.4.

The dimensions of each segment are determined from plots of the material properties for each leg such as shown in Figure 12.9.

12.2.3 Averaging Technique

A simple approach for estimating the efficiency can be obtained by using average values for the material properties of the module legs.[8] In this situation, the Thomson coefficient is equal to zero, and the

TABLE 12.2 Comparison between Iterative and Exact Modeling Techniques

	Iterative Technique	Exact Approach
Example I		
Efficiency (%)	2.94	2.9
Current (A)	1.24	1.22
A_n (cm^2)	0.0365	0.036
Example II		
Efficiency (%)	25.8	26
Current (A)	55	55
A_n (cm^2)	4.48	4.5
Example III		
Efficiency (%)	33.5	34
Current (A)	65.2	65
A_n (cm^2)	2.20	2.2

TABLE 12.3 Segmented Module from Ref. [7]

Segment	σ (S/cm)	κ (W/m K)	α (μV/K)	Temperature Span (K)
P_1	1886.8	4.636	154	720 –880
P_2	277.0	1.258	226	420 –720
P_3	1357.4	1.861	159	300 –420
N_1	246.9	1.342	231	420 –880
N_2	769.23	1.453	212	300 –420

efficiency is given by (for $A_p = 1$ cm^2)

$$\eta_t = \frac{I^2 R}{(\alpha_p - \alpha_n) T_h I + \frac{\Delta T}{L}(\kappa_p + A_n \kappa_n) - I^2 L \frac{1}{2}\left(\rho_p + \frac{\rho_n}{A_n}\right)} \tag{12.29}$$

TE devices are heat pumps and are Carnot efficiency-limited. Equation 12.29 can be rearranged as the product of the Carnot efficiency and the thermocouple efficiency as

$$\eta_t = \frac{T_h - T_c}{T_h} \frac{\sqrt{1 + Z\bar{T}} - 1}{\sqrt{1 + Z\bar{T}} + \frac{T_c}{T_h}} \tag{12.30}$$

TABLE 12.4 Results from the Test Structure Described in Ref. [7]

	From Ref. [7]	Iterative Technique
Length of P_1 (mm)	5.51	5.46
Length of P_2 (mm)	2.91	2.99
Length of P_3 (mm)	1.58	1.57
Length of N_1 (mm)	7.72	7.93
Length of N_2 (mm)	2.28	2.07
A_n (cm^2)	1.985	1.964
η (%)	11.48	11.48
I (A)	32.135	32.60

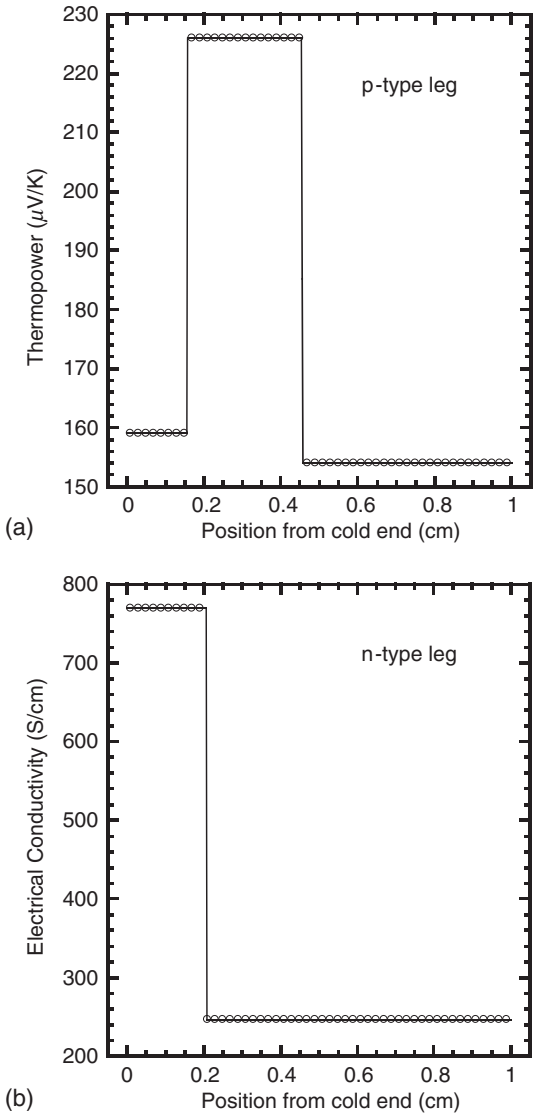

FIGURE 12.9 Profile of the (a) thermopower for the segmented p-type leg and (b) electrical conductivity for the n-type leg found from the iterative technique.

where $\bar{T} = \frac{1}{2}(T_h + T_c)$ and

$$Z = \left[\frac{(\alpha_p - \alpha_n)}{\sqrt{\rho_p \kappa_p} + \sqrt{\rho_n \kappa_n}} \right]^2 \tag{12.31}$$

is the figure-of-merit for the thermocouple. The efficiency is maximized for

$$A_n = \sqrt{\frac{\rho_n \kappa_p}{\rho_p \kappa_n}} \quad \text{and} \quad R = \sqrt{1 + \bar{T}Z}\left(\rho_p + \frac{\rho_n}{A_n}\right)L \tag{12.32}$$

or the load resistance is equal to $\sqrt{1 + \bar{T}Z}$ times the resistance of the module.

12.3 Multidimensional Analysis

The methods described in the previous sections assume the temperature and the electric potential distributions in each p- and n-leg of the TE module to be one-dimensional. Although this is generally a good assumption, there are configurations for which this assumption may not be valid. In this section, methods are presented that do not make this assumption and enable the analysis of legs, where the temperature and the electric potential distribution can be one-, two-, or three-dimensional. The organization of this section is as follows. First, the governing equations are described. Next, an efficient finite-volume (FV) method of solution is presented. This section concludes with computed results illustrating the multidimensional effects that can arise from heat transfer.

12.3.1 Governing Equations

The equations governing the multidimensional temperature and electrical potential distributions in TE materials under steady-state conditions and in the absence of an applied magnetic field are the energy equation and current flow equation given by Refs. [9–12]:

$$\nabla(\kappa\nabla T) + \rho\mathbf{J}^2 - T\mathbf{J}\cdot\left[\left(\frac{\partial\alpha}{\partial T}\right)\nabla T + (\nabla\alpha)_T\right] = 0 \tag{12.33}$$

$$\nabla\cdot\mathbf{J} = 0 \tag{12.34}$$

where

$$\mathbf{J} = -\sigma\left[\nabla\left(\frac{\mu}{\mathrm{e}} + V\right) + \alpha\nabla T\right] \tag{12.35}$$

$$\mathbf{q} = \alpha T\mathbf{J} - \kappa\nabla T \tag{12.36}$$

As in previous sections, the vector $\mathbf{J}$ is the electric current per unit area; the vector $\mathbf{q}$ is the heat transfer rate per unit area; T is temperature; κ is thermal conductivity at zero current; $\sigma = 1/\rho$ is electrical conductivity; ρ is electrical resistivity; α is the absolute Seebeck coefficient (thermopower); μ is the chemical potential; V is the electrostatic potential; and e is the charge of charged particles giving rise to the electrical current. Note that α, κ, σ, and ρ are functions of temperature.

Equation 12.33 to Equation 12.36 form a system of two coupled partial differential equations (PDEs) with two dependent variables, the temperature T and the electrical potential V. The boundary conditions (BCs) for the temperature are as follows. At all surfaces exposed to vacuum or gas, the BC imposed is either specified heat flux or specified heat transfer coefficient, i.e.

$$\mathbf{q}'' = \mathbf{q}''_{\mathbf{s}} \tag{12.37a}$$

or

$$\mathbf{q}'' = \mathbf{q}''_{\text{convection}} + \mathbf{q}''_{\text{radiation}} \tag{12.37b}$$

where

$$\mathbf{q}''_{\text{convection}} = h(T_{\mathrm{s}} - T_\infty) \tag{12.37c}$$

$$\mathbf{q}''_{\text{radiation}} = \epsilon\sigma' T_{\mathrm{s}}^4 + (1 - \alpha_{\text{op}})G_{\mathrm{s}} \approx h_{\text{rad}}(T_{\mathrm{s}} - T_\infty) \tag{12.37d}$$

In Equation 12.37a to d, T_{s} and $\mathbf{q}''_{\mathbf{s}}$ are, respectively, the temperature and heat flux at the surface of the leg exposed to vacuum or gas; T_{s} and $\mathbf{q}''_{\mathbf{s}}$ can be constant or function of position along the surface; T_∞ is the bulk mean temperature of the gas in the cavity between the p- and n-leg; h is the heat transfer coefficient and its value depends on the mode of convection such as natural or forced; ϵ and α_{op} are, respectively, the emissivity and the optical absorptivity of the leg surface; σ' is the

Stefan–Boltzmann constant; and h_{rad} is an effective radiation heat transfer coefficient. As written, Equation 12.37d neglects gas radiation, which should be modeled if there is water vapor or carbon dioxide in the gas. At all surfaces of the leg that are connected to the conducting plates, the BC imposed is either specified temperature or heat flux, i.e.

$$T = T_o \tag{12.38a}$$

or

$$\mathbf{q} = \mathbf{q}_o \tag{12.38b}$$

where T_o and $\mathbf{q}_o$ can be constant or function of position along the surface.

The BCs for the electrical potential are as follows. At all surfaces of the leg that are exposed to vacuum or gas, the current must be parallel to the surface, i.e.

$$\mathbf{J}\cdot\mathbf{n} = 0 \tag{12.39}$$

where $\mathbf{n}$ is a unit vector normal to the surface. At all surfaces of the leg that are connected to the conducting plates, the BC imposed is either specified electric potential or continuity of electric current, i.e.

$$V = V_o \tag{12.40a}$$

or

$$\mathbf{J} = \mathbf{J}_o \tag{12.40b}$$

In Equation 12.40a and b, V_o and $\mathbf{J}_o$ can be constant or function of position along the surface.

12.3.2 Numerical Method of Solution

Since the PDEs governing the temperature and electric potential distributions in TE materials given by Equation 12.33 to Equation 12.36 are not linear and the BCs given by Equation 12.37a to d to Equation 12.40a and b can be complicated functions of temperature and position, it is difficult to obtain exact solutions. However, there are a wide variety of numerical methods that can be used to generate approximate solutions to these equations (see for example, Refs. [13,14]). In this section, an efficient FV method that can handle complicated geometric shapes for TE legs and modules is presented.

Before presenting the FV method, it is noted that when solving Equation 12.33 to Equation 12.40a and b by any FV method, the FV method can be applied directly to those equations, or to an unsteady or time-dependent form of those equations. If a FV method is applied directly to Equation 12.33 to Equation 12.40a and b, then a system of nonlinear algebraic equations is obtained. Though this system can be solved iteratively by using the Newton–Raphson method or one of its variations, convergence requires the initial guess to be within the radius of convergence,[15] which is a difficult task. By applying a FV method to an unsteady form of the governing equations, initial guess can be constructed from physical considerations, and convergence is achieved when the time-derivative terms added to the governing equations approach zero within some prescribed tolerance. In addition to an easier path to convergence, the latter approach offers greater flexibility in constructing efficient algorithms. Thus, Equation 12.33 and Equation 12.34 are cast in *unsteady* form as follows:

$$\frac{1}{\gamma_T}\frac{\partial T}{\partial t} = \nabla(\kappa\nabla T) + f(T,V), \quad f(T,V) = \rho\mathbf{J}^2 - T\mathbf{J}\left[\left(\frac{\partial \alpha}{\partial T}\right)\nabla T + (\nabla\alpha)_T\right] \tag{12.41}$$

$$\frac{1}{\gamma_V}\frac{\partial V}{\partial t} = -\nabla\cdot\mathbf{J} \tag{12.42}$$

In the above equation, t denotes time or pseudo-time. Since time-accurate solutions are not of interest, γ_T and γ_V can take on any value that accelerates convergence to steady-state. By adding

a time-derivative term to Equation 12.33 and Equation 12.34, these equations are converted from elliptic to parabolic, but they revert back to elliptic once the time-derivative terms on the left-hand side of Equation 12.41 and Equation 12.42 vanish. Since the coefficient of the second derivative with respect to space coordinates must be positive for well-posed parabolic PDEs, the sign of γ_T and γ_V must be positive.

There are many FV methods that can be used to generate steady-state solutions to Equation 12.41 and Equation 12.42. These include explicit, implicit, and hybrid methods.[14] Explicit methods (e.g., methods in which the time derivatives are approximated by Runge–Kutta or Adams–Bashforth methods[16]) are extremely easy to derive and program, but they are conditionally stable. For the energy equation given by Equation 12.41 explicit methods can be used, because the stability criteria do not impose overly small time-step sizes so that convergence to the steady-state solution can be obtained with reasonable efficiency. However, for the electric-current equation given by Equation 12.42, the use of explicit methods does impose a very small time-step size, which will greatly slow convergence to steady-state. Since Equation 12.41 and Equation 12.42 are coupled, the smaller time-step size imposed by Equation 12.42 must be used. Thus, explicit methods are inefficient for solving Equation 12.41 and Equation 12.42. Implicit methods are much more stable than explicit methods; they are unconditionally stable for linear PDEs. By allowing for orders of magnitude larger time-step sizes, implicit methods converge much faster than explicit methods. However, implicit methods are more complicated to derive and program. In this study, a hybrid method is selected in which Equation 12.41 and Equation 12.42 are solved by using an explicit and implicit method, respectively. With the hybrid method, the maximum time-step that can be used is limited by the explicit method applied to Equation 12.41.

To illustrate the hybrid method for obtaining solutions to Equation 12.41 and Equation 12.42, consider a leg of a TE module with length L_x, and a rectangular cross-section of L_y by L_z (Figure 12.10). As with all FV methods, the derivation of the hybrid method for Equation 12.41 and Equation 12.42 along with BCs given by Equation 12.37a to d to Equation 12.40a and b involve the following three major steps:

(1) Discretize the domain;
(2) Replace the PDEs by algebraic equations;
(3) Specify the solution algorithm.

Each of these three steps is described below.

Discretize Domain: In this study, the domain of the problem (the rectangular leg shown in Figure 12.10) is discretized by dividing it into $(\mathrm{IL}-1)(\mathrm{JL}-1)(\mathrm{KL}-1)$ identical size cells as shown in Figure 12.11. The center of each of these cells is located at

$$x_i = (i - \tfrac{1}{2})\Delta x, \quad \Delta x = \mathrm{L}_x/(\mathrm{IL}-1), \quad i = 1, 2, \ldots, \mathrm{IL}-1 \tag{12.43a}$$

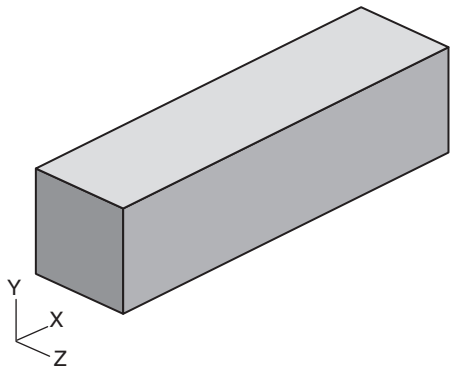

FIGURE 12.10 Leg of a TE module.

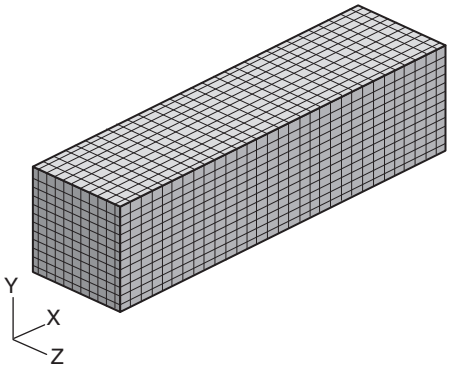

FIGURE 12.11 Leg divided into cells.

$$y_j = (j - \tfrac{1}{2})\Delta y, \quad \Delta y = L_y/(\mathrm{JL} - 1), \quad j = 1, 2, \ldots, \mathrm{JL} - 1 \tag{12.43b}$$

$$z_k = (k - \tfrac{1}{2})\Delta z, \quad \Delta z = L_z/(\mathrm{KL} - 1), \quad k = 1, 2, \ldots, \mathrm{KL} - 1 \tag{12.43c}$$

and each cell is bounded by the following coordinates:

$$x_{i-1/2} \quad \text{and} \quad x_{i+1/2}, \quad y_{j-1/2} \quad \text{and} \quad y_{j+1/2}, \quad z_{k-1/2} \quad \text{and} \quad z_{k+1/2} \tag{12.44}$$

In the above, IL, JL, and KL are integers, and their values determine the number and the shape of the cells in the domain. With such a simple discretization, the volume of each cell is

$$v_{i,j,k} = \Delta x \Delta y \Delta z \tag{12.45a}$$

and the areas of the faces bounding each cell are

$$A_{i-1/2,j,k} = A_{i+1/2,j,k} = \Delta y \Delta z \tag{12.45b}$$

$$A_{i,j-1/2,k} = A_{i,j+1/2,k} = \Delta x \Delta z \tag{12.45c}$$

$$A_{i,j,k-1/2} = A_{i,j,k+1/2} = \Delta x \Delta y \tag{12.45d}$$

If the cells in the domain are of unequal sizes, then Equation 12.45a to d must be modified to reflect the actual volumes and surface areas.

Discretize PDEs: With the domain discretized, the next step is to replace the governing equations by algebraic equations. This is accomplished in three steps. The first is to integrate the governing equations about each cell. For the (i, j, k)th cell, integration of the energy and electric-current equations given by Equation 12.41 and Equation 12.42 yields:

$$\int_{v_{i,j,k}} \left(\frac{1}{\gamma_T} \frac{\partial T}{\partial t} - \nabla(\kappa \nabla T) - f(T, V) \right) \mathrm{d}v = 0$$

$$\int_{v_{i,j,k}} \left(\frac{1}{\gamma_V} \frac{\partial V}{\partial t} + \nabla \cdot \mathbf{J} \right) \mathrm{d}v = 0$$

Upon noting that none of the cells deforms in time, the above equations become

$$\frac{v_{i,j,k}}{\gamma_T} \left(\frac{\partial \bar{T}}{\partial t} \right)_{i,j,k} = (\bar{f}v)_{i,j,k} + \int_{v_{i,j,k}} \nabla(\kappa \nabla T) \mathrm{d}v \tag{12.46}$$

$$\frac{\nu_{i,j,k}}{\gamma_V}\left(\frac{\partial \bar{V}}{\partial t}\right)_{i,j,k} = \int_{\nu_{i,j,k}} -\nabla\cdot\mathbf{J}\mathrm{d}\nu \tag{12.47}$$

$$\bar{T}_{i,j,k} = \frac{1}{\nu_{i,j,k}}\int_{\nu_{i,j,k}} T\mathrm{d}\nu, \quad \bar{V}_{i,j,k} = \frac{1}{\nu_{i,j,k}}\int_{\nu_{i,j,k}} V\mathrm{d}\nu, \quad \bar{f}_{i,j,k} = \frac{1}{\nu_{i,j,k}}\int_{\nu_{i,j,k}} f(T,V)\mathrm{d}\nu \tag{12.48}$$

where $\bar{T}$ and $\bar{V}$ are, respectively, the average temperature and electric potential in the (i,j,k)th cell. By invoking Gauss' theorem, the volume integrals involving divergence can be converted to surface integrals so that Equation 12.46 and Equation 12.47 become

$$\frac{\nu_{i,j,k}}{\gamma_T}\left(\frac{\partial \bar{T}}{\partial t}\right)_{i,j,k} = (\bar{f}\nu)_{i,j,k} + \int_{\partial\nu} (\kappa\nabla T)\cdot\mathbf{n}\mathrm{d}A \tag{12.49}$$

$$\frac{\nu_{i,j,k}}{\gamma_V}\left(\frac{\partial \bar{V}}{\partial t}\right)_{i,j,k} = \int_{\partial\nu} \mathbf{J}\cdot\mathbf{n}\mathrm{d}A \tag{12.50}$$

$$\mathbf{n} = \mathrm{n}_x\mathbf{i} + \mathrm{n}_y\mathbf{j} + \mathrm{n}_z\mathbf{k} \tag{12.51}$$

In the above equations, $\partial\nu$ denotes the surface bounding the cell; $\mathbf{n}$ denotes the unit vector normal to the cell surface and pointing away from the cell; and n_x, n_y, and n_z are directional cosines. Since each cell in Figure 12.11 are bounded by six faces, and the cell-face normals are aligned with the x, y, or z coordinate direction, Equation 12.49 and Equation 12.50 become

$$\frac{\nu_{i,j,k}}{\gamma_T}\left(\frac{\partial \bar{T}}{\partial t}\right)_{i,j,k} = (\bar{f}\nu)_{i,j,k} + \left(\sum_{\mathrm{face1}}^{\mathrm{face6}} \overline{\kappa\nabla T}\cdot\mathbf{n}_{\mathrm{face}}\right)_{i,j,k} \tag{12.52a}$$

$$\frac{\nu_{i,j,k}}{\gamma_V}\left(\frac{\partial \bar{V}}{\partial t}\right)_{i,j,k} = -\left(\sum_{\mathrm{face1}}^{\mathrm{face6}} \bar{\mathbf{J}}\cdot\mathbf{n}_{\mathrm{face}}\right)_{i,j,k} \tag{12.53a}$$

where

$$\begin{aligned}\sum_{\mathrm{face1}}^{\mathrm{face6}} \overline{\kappa\nabla T}\cdot\mathbf{n}_{\mathrm{face}} = {} & \left(\overline{\kappa\frac{\partial T}{\partial x}}A\right)_{i+\frac{1}{2},j,k} - \left(\overline{\kappa\frac{\partial T}{\partial x}}A\right)_{i-\frac{1}{2},j,k} + \left(\overline{\kappa\frac{\partial T}{\partial y}}A\right)_{i,j+\frac{1}{2},k} - \left(\overline{\kappa\frac{\partial T}{\partial y}}A\right)_{i,j-\frac{1}{2},k} \\ & + \left(\overline{\kappa\frac{\partial T}{\partial z}}A\right)_{i,j,k+\frac{1}{2}} - \left(\overline{\kappa\frac{\partial T}{\partial z}}A\right)_{i,j,k-\frac{1}{2}}\end{aligned} \tag{12.52b}$$

$$\begin{aligned}\sum_{\mathrm{face1}}^{\mathrm{face6}} \bar{\mathbf{J}}\cdot\mathbf{n}_{\mathrm{face}} = {} & (\bar{J}_xA)_{i+\frac{1}{2},j,k} - (\bar{J}_xA)_{i-\frac{1}{2},j,k} + (\bar{J}_yA)_{i,j+\frac{1}{2},k} - (\bar{J}_yA)_{i,j,-\frac{1}{2},k} \\ & + (\bar{J}_zA)_{i,j,k+\frac{1}{2}} - (\bar{J}_zA)_{i,j,k-\frac{1}{2}}\end{aligned} \tag{12.53b}$$

$$J_\phi = -\sigma\left[\frac{\partial}{\partial\phi}\left(\frac{\mu}{e}+V\right) + \alpha\frac{\partial T}{\partial\phi}\right], \qquad \phi = x,y,z \tag{12.53c}$$

In the above equations, the bars over J_x, J_y, J_z, and the derivatives of T denote averages over the respective cell faces. In this study, all derivatives in the fluxes across the faces as well as those appearing in the source term $\bar{f}$ are approximated by second-order accurate central differences. The fluxes in the x direction are approximated as follows

$$\left(\overline{\kappa\frac{\partial T}{\partial x}}A\right)_{i+\frac{1}{2},j,k} \approx (\bar{\kappa}A)_{i+\frac{1}{2},j,k}\frac{\bar{T}_{i+1,j,k} - \bar{T}_{i,j,k}}{\Delta x} \tag{12.52c}$$

$$\left(\overline{\kappa\frac{\partial T}{\partial x}}A\right)_{i-\frac{1}{2},j,k} \approx (\bar{\kappa}A)_{i-\frac{1}{2},j,k}\frac{\bar{T}_{i,j,k}-\bar{T}_{i-1,j,k}}{\Delta x} \tag{12.52d}$$

$$(\bar{J}_xA)_{i+\frac{1}{2},j,k} = -(\bar{\sigma}A)_{i+\frac{1}{2},j,k}\left[\frac{\left(\frac{\bar{\mu}}{e}+\bar{V}\right)_{i+1,j,k}-\left(\frac{\bar{\mu}}{e}+\bar{V}\right)_{i,j,k}}{\Delta x}+\bar{\alpha}_{i+\frac{1}{2},j,k}\frac{\bar{T}_{i+1,j,k}-\bar{T}_{i,j,k}}{\Delta x}\right]$$

$$= -(\bar{\sigma}A)_{i+\frac{1}{2},j,k}\left[\delta_x\left(\frac{\bar{\mu}}{e}+\bar{V}\right)_{i+\frac{1}{2},j,k}+\bar{\alpha}_{i+\frac{1}{2},j,k}\delta_x\bar{T}_{i+\frac{1}{2},j,k}\right] \tag{12.53d}$$

$$(\bar{J}_xA)_{i-\frac{1}{2},j,k} = -(\bar{\sigma}A)_{i-\frac{1}{2},j,k}\left[\frac{\left(\frac{\bar{\mu}}{e}+\bar{V}\right)_{i,j,k}-\left(\frac{\bar{\mu}}{e}+\bar{V}\right)_{i-1,j,k}}{\Delta x}+\bar{\alpha}_{i-\frac{1}{2},j,k}\frac{\bar{T}_{i,j,k}-\bar{T}_{i-1,j,k}}{\Delta x}\right]$$

$$= -(\bar{\sigma}A)_{i-\frac{1}{2},j,k}\left[\delta_x\left(\frac{\bar{\mu}}{e}+\bar{V}\right)_{i-\frac{1}{2},j,k}+\bar{\alpha}_{i-\frac{1}{2},j,k}\delta_x\bar{T}_{i-\frac{1}{2},j,k}\right] \tag{12.53e}$$

$$\bar{\psi}_{i\pm\frac{1}{2},j,k} = \tfrac{1}{2}(\bar{\psi}_{i\pm1,j,k}+\bar{\psi}_{i,j,k}), \qquad \psi = \kappa, \sigma, \alpha \tag{12.54}$$

The derivatives of V, T, and μ in the source terms are approximated as follows:

$$\left(\frac{\partial \Phi}{\partial x}\right)_{i,j,k} \approx \frac{\Phi_{i+\frac{1}{2},j,k}-\Phi_{i-\frac{1}{2},j,k}}{\Delta x}, \quad \Phi_{i\pm\frac{1}{2},j,k} = \Phi_{i\pm1,j,k}+\Phi_{i,j,k}, \quad \Phi = V, T, \mu \tag{12.55}$$

The fluxes and derivatives in the y direction and z direction are approximated in a similar manner.

For all cell faces that are on the boundary of the domain, the appropriate BC given by Equation 12.37a to d to Equation 12.40a and b must be applied. For example, the heat flux at all surfaces of the TE leg exposed to gas must satisfy Equation 12.37a to d. Also, the electric potential there must be such that the electric current only flows along the surface with no component perpendicular to the surface as stipulated by Equation 12.39.

The time derivative in Equation 12.52a is approximated by the conditionally stable, first-order accurate in time, Euler explicit method. Since only the final steady-state solution is of interest, the lowest-order accurate time-difference formula is used. With the Euler explicit method, Equation 12.52a becomes

$$\bar{T}^{n+1}_{i,j,k} = \bar{T}^{n}_{i,j,k}+\gamma_T\Delta t\left(\bar{f}^{n}_{i,j,k}\right)+\frac{\gamma_T\Delta t}{\nu_{i,j,k}}\left(\sum_{\text{face1}}^{\text{face6}}\overline{\kappa\nabla T}\cdot\mathbf{n}_{\text{face}}\right)^{n}_{i,j,k} \tag{12.56}$$

In the above equation, the superscript n denotes data at the nth time level (i.e., $t^n = n\Delta t$; Δt is taken to be a constant), where the solution is assumed to be known, and the superscript $(n+1)$ denotes data at the $(n+1)$th time level (i.e., $t^{n+1} = t^n + \Delta t$), where the solution is unknown and to be determined. Equation 12.56 is the algebraic representation of the energy equation given by Equation 12.41, and it is valid for all cells whose faces do not coincide with a boundary. For those cells with faces that coincide with a boundary, appropriate BC for the temperature or heat flux must be imposed. Thus, we rewrite Equation 12.56 as follows so that it is valid for all cells:

$$\bar{T}^{n+1}_{i,j,k} = \bar{T}^{n}_{i,j,k}+\gamma_T\Delta t\left(\bar{f}^{n}_{i,j,k}\right)+\frac{\gamma_T\Delta t}{\nu_{i,j,k}}\left(\sum_{\text{face1}}^{\text{face6}}\overline{-q''}\mathbf{n}_{\text{face}}\right)^{n}_{i,j,k} \tag{12.57a}$$

where

$$\mathbf{q}'' = -\kappa \nabla T \quad \text{for all faces that do not see gas} \tag{12.57b}$$

$$\mathbf{q}'' = \mathbf{q}''_{\text{convection}} + \mathbf{q}''_{\text{radiation}} \quad \text{per Equation 12.37a to d for faces that see gas} \tag{12.57c}$$

For Equation 12.53a the first-order accurate in time, Euler implicit method is used to approximate the time derivative term, which is numerically more stable than the Euler explicit method. Again, only the lowest-order accurate in time method is used because only the steady-state solution is of interest. By using the Euler implicit method, Equation 12.53a becomes

$$\bar{V}^{n+1}_{i,j,k} = \bar{V}^{n}_{i,j,k} - \frac{\gamma_V \Delta t}{\nu_{i,j,k}} \left(\sum_{\text{face1}}^{\text{face6}} \mathbf{J} \cdot \mathbf{n}_{\text{face}} \right)^{n+1}_{i,j,k} \tag{12.58}$$

Unlike Equation 12.56, the right-hand side of Equation 12.58 involves derivatives of $\bar{T}$ and $\bar{V}$ at the $(n+1)$th time level, where they are unknown instead of the nth time level, where they are known. The unknown $\bar{T}^{n+1}$ in Equation 12.58 can be obtained from Equation 12.57a to c to be explained later, but the unknown $\bar{V}^{n+1}$ requires the solution of a system on linear equations of order $m = (\text{IL} - 1)(\text{JL} - 1)(\text{KL} - 1)$ and of bandwidth $w = \min[(\text{IL} - 1)(\text{JL} - 1), (\text{IL} - 1)(\text{KL} - 1), (\text{JL} - 1)(\text{KL} - 1)]$. The operation count needed to solve this system of equations can be reduced by orders of magnitude if a method known as approximate factorization (AF) is used.[14] To implement the AF method, Equation 12.58 is rewritten in the following operator form:

$$\theta \Delta \bar{V}^{n}_{i,j,k} + (\phi_x + \phi_y + \phi_z) \Delta \bar{V}^{n}_{i,j,k} = \phi_T \tag{12.59a}$$

where

$$\theta = \frac{\nu_{i,j,k}}{\gamma_V \Delta t} \tag{12.59b}$$

$$\Delta \bar{V}^{n}_{i,j,k} = \bar{V}^{n+1}_{i,j,k} - \bar{V}^{n}_{i,j,k} \tag{12.59c}$$

$$\phi_x = -\left[(\bar{\sigma} A \delta_x)_{i+\frac{1}{2},j,k} - (\bar{\sigma} A \delta_x)_{i-\frac{1}{2},j,k} \right] \tag{12.59d}$$

$$\phi_y = -\left[\left(\bar{\sigma} A \delta_y \right)_{i,j+\frac{1}{2},k} - \left(\bar{\sigma} A \delta_y \right)_{i,j-\frac{1}{2},k} \right] \tag{12.59e}$$

$$\phi_z = -\left[(\bar{\sigma} A \delta_z)_{i,j,k+\frac{1}{2}} - (\bar{\sigma} A \delta_z)_{i,j,k-\frac{1}{2}} \right] \tag{12.59f}$$

$$\phi_T = -(\phi_x + \phi_y + \phi_z) \left(\frac{\bar{\mu}^{n+1}}{e} + \bar{V}^{n} \right)_{i,j,k} - (\phi'_x + \phi'_y + \phi'_z) \bar{T}^{n+1}_{i,j,k} \tag{12.59g}$$

$$\phi'_x = -\left[(\bar{\sigma} \alpha A \delta_x)_{i+\frac{1}{2},j,k} - (\bar{\sigma} \alpha A \delta_x)_{i-\frac{1}{2},j,k} \right] \tag{12.59h}$$

$$\phi'_y = -\left[\left(\bar{\sigma} \alpha A \delta_y \right)_{i,j+\frac{1}{2},k} - \left(\bar{\sigma} \alpha A \delta_y \right)_{i,j-\frac{1}{2},k} \right] \tag{12.59i}$$

$$\phi'_z = -\left[(\bar{\sigma} \alpha A \delta_z)_{i,j,k+\frac{1}{2}} - (\bar{\sigma} \alpha A \delta_z)_{i,j,k-\frac{1}{2}} \right] \tag{12.59j}$$

Equation 12.59a can be approximately factored as follows[17]:

$$(\theta + \phi_x)\theta^{-1}(\theta + \phi_y)\theta^{-1}(\theta + \phi_z)\Delta\bar{V}^n_{i,j,k} = \phi_T \tag{12.60}$$

Note that at steady-state, $\Delta\bar{V}^n_{i,j,k} = 0$ so that the errors introduced by the AF vanish. Equation 12.60 can be split into the following three one-dimensional operators:

$$(\theta + \phi_x)\Delta\bar{V}^*_{i,j,k} = \phi_T \tag{12.61a}$$

$$(\theta + \phi_y)\Delta\bar{V}^{**}_{i,j,k} = \theta\Delta\bar{V}^*_{i,j,k} \tag{12.61b}$$

$$(\theta + \phi_z)\Delta\bar{V}^n_{i,j,k} = \theta\Delta\bar{V}^{**}_{i,j,k,} \tag{12.61c}$$

$$\bar{V}^{n+1}_{i,j,k} = \bar{V}^n_{i,j,k} + \Delta\bar{V}^n_{i,j,k} \tag{12.61d}$$

Equation 12.61a to d forms systems of linear equations with tridiagonal coefficient matrices that can be solved very efficiently by the Thomas algorithm.[14] Also, the order of the matrices is now (IL − 1), (JL − 1), or (KL − 1) instead of [(IL − 1)(JL − 1)(KL − 1)].

Specify Solution Algorithm: With the domain discretized and the governing equations replaced by algebraic equations, the solution algorithm can now be described as follows:

1. Input geometry of leg by specifying L_x, L_y, and L_z.
2. Input TE material properties by specifying κ, σ, α, and ρ as a function of temperature.
3. Specify BCs for $\bar{T}$ and $\bar{V}$ via Equation 12.37a to d to Equation 12.40a and b.
4. Calculate cell volumes, cell face areas, and spacing between cell centers by using Equation 12.43a to c and Equation 12.45a to d.
5. Specify γ_T, γ_V, and the time-step size (Δt) to be used that ensure numerical stability, and rapid convergence to steady-state solutions.
6. Set the time level index $n = 0$.
7. Specify the initial condition or initial guess for $\bar{T}$ and $\bar{V}$ at every cell (i.e., $\bar{T}^n_{i,j,k}$ and $\bar{V}^n_{i,j,k}$ at $n = 0$). $\bar{T}^n_{i,j,k}$ and $\bar{V}^n_{i,j,k}$ at $n = 0$ can be constant or linearly interpolated from their values on the boundaries.
8. Calculate TE material properties (κ, σ, α, and ρ) at every cell based on $\bar{T}^n_{i,j,k}$.
9. Calculate $\bar{T}$ at every cell at the $(n + 1)$th time level ($\bar{T}^{n+1}_{i,j,k}$) by using Equation 12.57a to c.
10. Calculate TE material properties (κ, σ, α, and ρ) at every cell based on $\bar{T}^{n+1}_{i,j,k}$.
11. Calculate $\bar{V}$ at every cell at the $(n + 1)$th time level ($\bar{V}^{n+1}_{i,j,k}$) by using Equation 12.61a to d, where $\bar{T}^{n+1}_{i,j,k}$ is from Step nine.
12. Examine convergence. If $\dfrac{|\bar{T}^{n+1}_{i,j,k} - \bar{T}^n_{i,j,k}|}{|\bar{T}^{n+1}_{i,j,k}|} < \varepsilon_T$ and $\dfrac{|\bar{V}^{n+1}_{i,j,k} - \bar{V}^n_{i,j,k}|}{|\bar{V}^{n+1}_{i,j,k}|} < \varepsilon_V$ at every cell, then the solution at the $(n + 1)$th time level is taken to be converged. Otherwise, set n to $n + 1$ and repeat Steps 9 to 12. In the above, the convergence criteria, ε_T and ε_V, can be set as 10^{-5} or some smaller number.

12.3.3 Computed Results and Discussions

In this section, the numerical method presented in the above is applied to study the temperature and electric potential distributions in the leg of a TE module depicted in Figure 12.12. Table 12.5 summarizes the four cases simulated to illustrate how heat transfer can produce multidimensional effects. As noted in Figure 12.12 and Table 12.5, the TE leg investigated is rectangular in shape and has length L_x (10 mm) and cross-sectional area L_yL_z (25 mm^2). The temperature at the hot end of the leg ($x = 0$) is maintained at $T_h - \Delta T(y/L_y)$, where T_h is 900 K and ΔT is either 0 K or 50 K. ΔT is intended to examine the effects

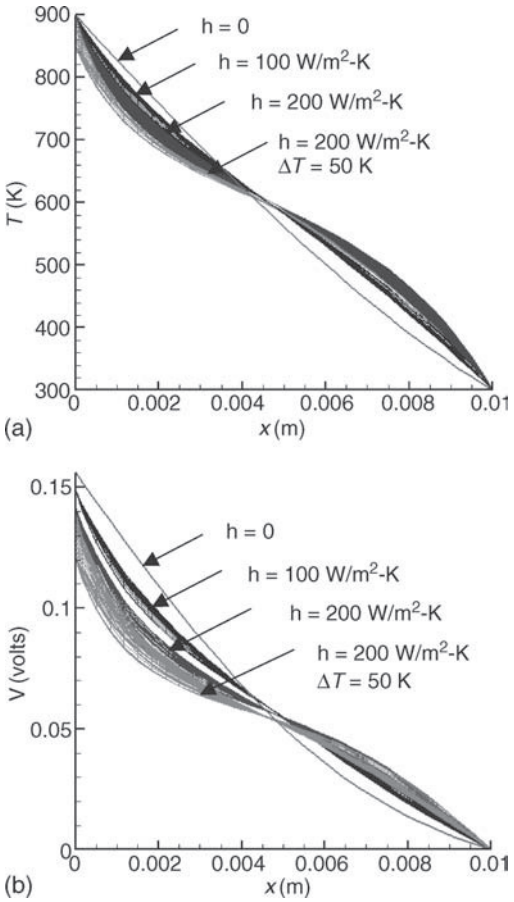

FIGURE 12.12 **(See color insert following page 31-12.)** Predicted T and V distributions along x in an $x-y$ plane midway between the ends in z direction. Multiple lines indicate variations in T and V in the $x-y$ plane.

of nonuniform temperature distribution at the base of the TE leg, which can be appreciable if the cross-sectional area of the leg is large and if the heat transfer rate to or from the cold and hot sources are appreciable. The temperature at the cold end of the TE leg ($x = L_x$) is maintained at T_c, which was set to be a constant at the ambient temperature of 300 K. The temperature BC for all surfaces exposed to the gas was specified by using Equation 12.37a to d, where h is either 0 W/m^2 K, 100 W/m^2 K, or 200 W/m^2 K, representing contributions from both natural convection and radiation heat transfer. T_∞ is set to be the arithmetic average of T_h and T_c. The BCs used for the electric potential are as follows. At the hot end of the TE leg ($x = 0$), current is extrapolated, whereas at the cold end ($x = L_x$), the electric potential is set to zero. On all surfaces of the TE leg exposed to the gas, Equation 12.39 is imposed. In all cases, the TE

TABLE 12.5 Summary of Cases Simulated

Case	T_h (K)	T_c (K)	ΔT (K)	h (W/m^2 K)	L_x, L_y, L_z (mm)
1	900	300	0	0	10, 5, 5
2	900	300	0	100	10, 5, 5
3	900	300	0	200	10, 5, 5
4	900	300	50	200	10, 5, 5

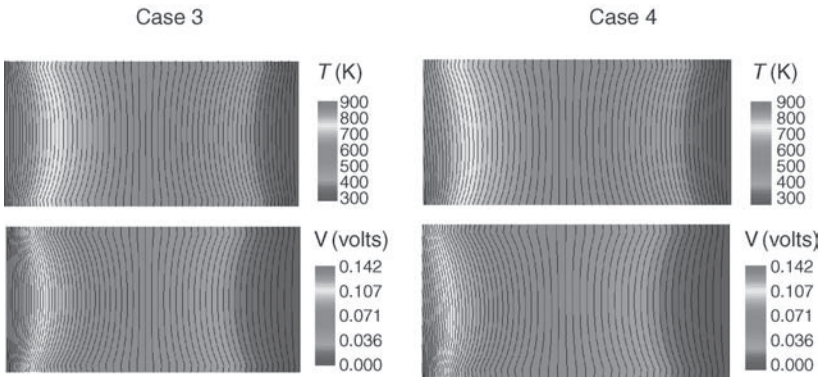

FIGURE 12.13 **(See color insert following page 31-12.)** Predicted T and V distributions in the middle $x-y$ plane.

material (n-type) has the following temperature-dependent properties

$$\alpha = -297.7 + 1.855T - 0.0061604T^2 + 6.4013 \times 10^{-6}T^3 - 2.1847 \times 10^{-9}T^4 \ (\mu V/K)$$

$$\sigma = 116.83 + 13561\ e^{-0.0068336T} \ (\text{S/cm})$$

$$\kappa = 0.23912 + 609.95/T - 838.3/T^2 \ (\text{W/m K})$$

The results generated for Cases 1 to 4 are plotted in Figure 12.12 through Figure 12.14. In Figure 12.12, it can be seen that for Case 1 with $h = 0$ (i.e., no heat loss from the four sides of the TE leg), the temperature profile is nearly linear. This is because, the effect of having a thermal conductivity that decreases with temperature is offset by temperature increases from heat generation due to electric current flow. For Case 1, T and V are onedimensional (i.e., they are only functions of x), and serve as a reference for comparing with cases for which there are heat transfer from the four sides of the TE leg exposed to gas.

For Case 2 with $h = 100$ W/m^2 K, it can be seen from Figure 12.12 and Figure 12.13 that the T and V become three-dimensional (3-D).

Since $T_\infty = (T_h + T_c)/2$, the TE material losses "heat" when its surface temperature is higher than T_∞ and gains "heat" when its surface temperature is lower than T_∞. Thus, temperature near the hot end is lower than the 1-D prediction, whereas the temperature near the cool end is higher than the 1-D

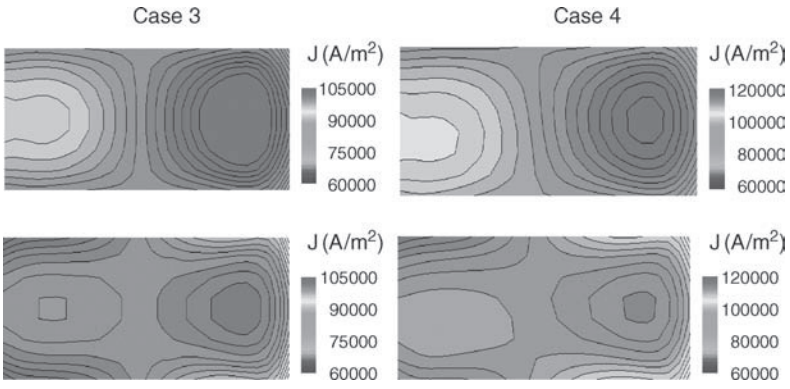

FIGURE 12.14 **(See color insert following page 31-12.)** Predicted magnitude of the electric current in the middle $x-y$ plane (top) and in a plane near the surface exposed to gas (bottom).

prediction. This observation can be discerned in Figure 12.12 by comparing the results obtained for Cases 1 and 2. Once the temperature becomes multidimensional, Figure 12.12 and Figure 12.13 show that the electric potential distribution becomes multidimensional. By increasing the heat transfer to- or from the four sides of the TE leg exposed to gas (e.g., from $h = 100$ W/m^2 K of Case 2 to $h = 200$ W/m^2 K of Case 3), Figure 12.12 shows the temperature near the hot end to be lowered more and the temperature near the cold end to be increased more. In Case 4, the hot end is assumed to have a linear temperature variation of 50 K, which produces a nonsymmetric distribution of T and V. The effect of the multidimensionality in T and V is to make the electric current flow to be nonuniform throughout the TE material as shown in Figure 12.14. Not shown here is that when the gradients of T and V have opposite signs, the distribution of T and V differ markedly from those shown in Figure 12.12.

Nomenclature

Symbol	Quantity	Symbol	Quantity
A_n	cross-sectional area of the n-type leg	T_h	temperature on the hot-side of the module
A_p	cross-sectional area of the p-type leg	T_n	temperature of the n-type leg
E	electronic charge (-1.602×10^{-19} C)	T_p	temperature of the p-type leg
$\mathbf{E}$	electric field	V	electrostatic potential
h	heat transfer rate	$\mathbf{W}$	energy flux
I	electrical current	$\mathbf{X}_j$	force giving rise to the flows
$\mathbf{J}$	electrical current density	α	thermoelectric (TE) power
$\mathbf{J}_i$	flow of particles or energy	η_n	efficiency of the n-type leg
$\mathbf{J}_q$	particle current density	η_p	efficiency of the p-type leg
$\mathbf{J}_s$	entropy current density	η_t	thermodynamic efficiency
L_{ij}	Onsager parameters linking forces and flows	κ	thermal conductivity
P_o	output electrical power from the module	κ_n	thermal conductivity of the n-type leg
$\mathbf{q}$	heat flux	κ_p	thermal conductivity of the p-type leg
$\mathbf{q}''$	surface heat flux	μ	chemical potential
Q_c	heat flow on the cold-side of the module	$\bar{\mu}$	electrochemical potential
Q_h	heat flow on the hot-side of the module	ρ	electrical resistivity
R_L	electrical load resistance	τ_n	Thomson coefficient of the n-type leg
S^*	transport entropy per particle	τ_p	Thomson coefficient of the p-type leg
T	temperature	x, y, z	position variables
T_c	temperature on the cold-side of the module		

Acknowledgment

Financial support from the Office of Naval Research and the Department of Defense MURI program is gratefully acknowledged.

References

1. Onsager, L., Reciprocal relations in irreversible processes, I, *Phys. Rev.*, 37, 405–426, 1931.
2. Domenicali, C.A., Irreversible thermodynamics of TE effects in inhomogeneous, anisotropic media, *Phys. Rev.*, 92(4), 877–881, 1953.
3. Sherman, B., Heikes, R.R., and Ure, R.W. Jr., Calculation of efficiency of TE devices, *J. Appl. Phys.*, 31(1), 1–16, 1960.

4. Buist, R.J., Calculation of Peltier device performance, *CRC Handbook of TEs*, pp. 143–155. CRC Press, Inc., New York, chap 14, 1995.
5. Hogan, T., Loo, S., Guo, F., and Short, J., Measurement techniques for TE materials and modules, *Materials Research Society Symposium Proceedings*, Vol. 793, pp. 405–411, 2004.
6. Mahan, G.D., Inhomogeneous TEs, *J. Appl. Phys.*, 70, 8, 4551, 1991.
7. Swanson, B.W., Somers, E.V., and Heikes, R.R., Optimization of a sandwiched TE device, *J. Heat Transfer*, 83, 77–82, 1961.
8. Ioffe, A.F., *Semiconductor Thermoelements and TE Cooling*, Infosearch Limited, London, 1957.
9. D.M.Rowe, ed., *CRC Handbook of TEs*, CRC Press, Boca Raton, FL, 1995.
10. De Groot, S.R. and Mazur, P., *Nonequilibrium Thermodynamics*. Dover, New York, 1984, originally published by North-Holland Publishing Company, Amsterdam, 1962.
11. Callen, H.B., *Thermodynamics and an Introduction to Thermostatics*, 2nd ed. Wiley, New York, 1985.
12. Mahan, G.D., Density variations in TEs, *J. Appl. Phys.*, 87, 10, 7326–7332, 2000.
13. Lapidus, L. and Pinder, G.F., *Numerical Solution of Partial Differential Equations in Science and Engineering*, Wiley, New York, 1982.
14. Tannehill, J.C., Anderson, D.A., and Pletcher, R.H., *Computational Fluid Dynamics and Heat Transfer*, 2nd ed. Taylor and Francis, Washington, DC, 1997.
15. Ralston, A. and Rabinowitz, P., *A First Course in Numerical Analysis*, 2nd ed. McGraw-Hill Book Co., New York, 1978.
16. Lambert, J.D., *Computational Methods in Ordinary Differential Equations*. Wiley, Chichester, 1973.
17. Shih, T.I-P. and Chyu, W.J., Approximate-factorization with source terms, *AIAA J.*, 29, 1759–1760, 1991.